SPIKING NEURAL NETWORKS FOR BREAST CANCER CLASSIFICATION IN A DIELECTRICALLY HETEROGENEOUS BREAST

M. O'Halloran, B. McGinley, R. C. Conceicao, F. Morgan E. Jones and M. Glavin [†]

College of Engineering and Informatics
National University of Ireland Galway
University Road, Galway, Ireland

Abstract—The considerable overlap in the dielectric properties of benign and malignant tissue at microwave frequencies means that breast tumour classification using traditional UWB Radar imaging algorithms could be very problematic. Several studies have examined the possibility of using the Radar Target Signature (RTS) of a tumour to classify the tumour as either benign or malignant, since the RTS has been shown to be influenced by the size, shape and surface texture of tumours. The main weakness of existing studies is that they mainly consider tumours in a 3D dielectrically homogenous or 2D heterogeneous breast model. In this paper, the effects of dielectric heterogeneity on a novel Spiking Neural Network (SNN) classifier are examined in terms of both sensitivity and specificity, using a 3D dielectrically heterogeneous breast model. The performance of the SNN classifier is compared to an existing LDA classifier. The effect of combining conflicting classification readings in a multi-antenna system is also considered. Finally and importantly, misclassified tumours are analysed and suggestions for future work are discussed.

1. INTRODUCTION

Two criteria determine the effectiveness of any breast cancer screening methodology: specificity and sensitivity. Specificity is defined as the proportion of patients correctly identified as not having breast cancer. Conversely, sensitivity is defined as the proportion of patients correctly identified as having breast cancer. Therefore, a good screening methodology must have both high sensitivity and high specificity. The current standard screening method for detecting non-palpable early stage breast cancer is X-ray mammography. Despite the fact that X-ray mammography provides high resolution images using relatively low radiation doses, its limitations are well documented [1]. In younger women in particular, breast tissue typically presents a higher dense-to-fatty tissue ratio and malignancies occurring in dense-tissue breasts are statistically more likely to be missed by X-ray mammography [2]. In the US, between 4%–34% of all breast cancers are missed by conventional mammography [3], while 70% of all malignancies identified are found to be benign after biopsy [4]. These false positive diagnoses result in unnecessary biopsies, causing considerable distress to the patient and an unnecessary financial burden on the health service [4, 5].

UWB Radar has been proposed as a method to detect early stage breast cancer [6–9]. Several studies have examined the use of UWB Radar to classify breast cancer as benign or malignant. This classification approach is based on the Radar Target Signature, which reflect the size, shape and surface texture of the tumour. Benign tumours typically have smooth surfaces and have spherical, oval or at least well-circumscribed contours. Conversely, malignant tumours usually present rough and complex surfaces with spicules or microlobules, and their shapes are typically irregular, ill-defined and asymmetric [10]. These tumour characteristics are generally reflected in the details of the RTS and can be used in classifiers. Several classifiers and classification architectures have been investigated [11–16]. However, the performance of the majority of these algorithms in a realistic 3D dielectrically heterogeneous scenario has not been examined. Therefore, the contributions of this paper are as follows:

- Evaluation of a novel Spiking Neural Network (SNN) classifier in a 3D dielectrically heterogenous breast model;
- Comparison of SNN classifier with existing Linear Discriminant Analysis (LDA) classifier;
- Analysis of misclassified tumours.

The structure of the remainder of the paper is as follows: Section 2 describes the generation of realistic tumour models, including dielectric

heterogeneity and corresponding FDTD simulations; Section 3 describes the SNNs and the Genetic Algorithm used for SNN training; Section 4 describes the experimental setup, while Section 5 describes the results and corresponding conclusions.

2. MODELING

2.1. Gaussian Random Spheres and Dielectric Heterogeneity

Shape and texture of the surface of a tumour are two of the most important characteristics used to differentiate between a benign and a malignant tumour. The tumour models used in this paper are based on the Gaussian Random Spheres (GRS) method [17, 18]. GRS can be modified mathematically to model both malignant and benign tumours by varying the mean radius α and the covariance function of the logarithmic radius. The shape is determined by the radius vector, $\mathbf{r} = r(\theta, \psi)$, described in spherical coordinates (r, θ, ψ), by the spherical harmonics series for the logradius $s = s(\theta, \psi)$:

$$r(\theta, \psi) = \alpha \exp\left[s(\theta, \psi) - \frac{1}{2}\beta^2\right] \tag{1}$$

$$s(\theta, \psi) = \sum_{l=0}^{\infty} \sum_{m=-l}^{l} s_{lm} Y_{lm}(\theta, \psi) \tag{2}$$

In the equations above, β is the standard deviation of the logradius, s_{lm} are the spherical harmonic coefficients and Y_{lm} are the orthonormal spherical harmonics. Three different tumour models at two different sizes are considered in this paper. Malignant tumours are represented by spiculated GRS, whereas benign tumours are modelled by smooth and macrolobulated GRS. Macrolobulated and smooth GRS are obtained by varying the correlation angle from low to high. Spiculated GRS are obtained by adding 3, 5 or 10 spicules to smooth GRS. The average radius of all types of spheres are 2.5 and 7.5 mm. Between all sizes and shapes, the number of tumour models developed was 160 (80 malignant and 80 benign).

In order to account for dielectric heterogeneity, fibroglandular tissue is introduced into the FDTD models. Portions of fibroglandular tissue, extracted from the UWCEM Breast Phantom Repository, are introduced into the FDTD model (phantom ID 071904). For the Hetero I simulations, a single piece of fibroglandular tissue is added to the FDTD models, positioned at one of ten random locations surrounding the tumour. For the Hetero II simulations, two independent portions of fibroglandular tissue are positioned at two of ten random locations
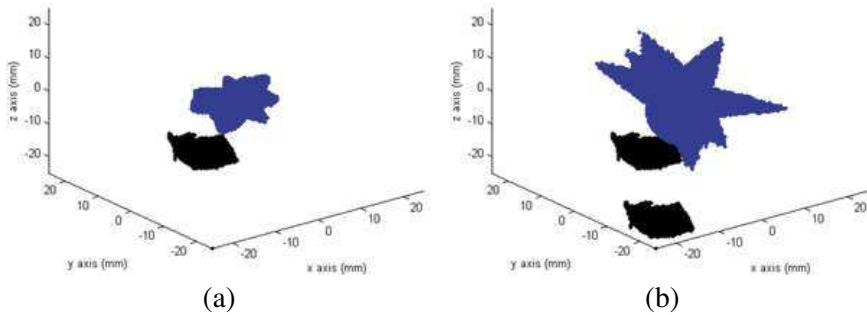
Figure 1. (a) Example of a Hetero I model, and (b) a Hetero II model. The tumour is shown in blue, while the fibroglandular tissue is shown in black.

around the tumour. Examples of Hetero I and Hetero II models are shown in Figure 1.

2.2. FDTD Model

The tumours (80 of size 2.5 mm and 80 of size 7.5 mm) are placed in a 3D Finite-Difference Time-Domain (FDTD) model. The FDTD model has a 0.5 mm cubic grid resolution and the backscattered signals were generated through a Total-Field/Scattered-Field (TF/SF) structure, in which the tumours and fibroglandular tissue are completely embedded in the Total Field (TF) [14, 16]. The TF/SF region has the following dimensions: the Scattered Field (SF) is a square geometric prism with square bases measuring 153.5 mm on the side and the height measuring 137.5 mm. The TF is located at the centre of the SF and is represented by a 50 mm-sided cube (the origin of the SF and the TF are at the point (0,0,0) mm). The dielectric properties of both adipose, fibroglandular, and cancerous breast tissue are incorporated using a Debye model, based on the dielectric properties established by Lazebnik et al. [19, 20]. The TF/SF region is terminated with a 6 mm-layer Uniaxial Perfectly Matched Layer (UPML) which suppresses any boundary reflections [21].

A pulsed plane wave is transmitted towards the target from four different equidistant angles ($0°, 90°, 180°, 270°$) and the resulting cross-polarized backscatter is recorded and analysed from four observation points located at: $(0, 0, -74)$, $(-74, 0, 0)$, $(0, 0, 74)$ and $(74, 0, 0)$ mm in (x, y, z) axes. The incident pulse is a modulated Gaussian pulse with center frequency at 6 GHz where the $1/e$ full temporal width of the Gaussian envelope was 160 ps. For two transmitters, the pulse is
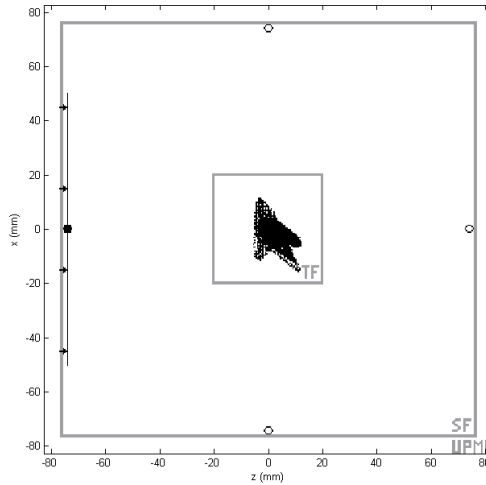
Figure 2. Cross-section of the 3D FDTD space lattice partitioned into Total Field (TF), Scattered Field (SF) and UPML regions, for a homogeneous breast model. The target, a spiculated tumour located at the centre of the TF in this example, is illuminated by a pulsed plane wave propagating in the $+z$ direction (represented by a dark line) and backscatter is recorded at the first observer location: $(0, 0, -74)$ mm (represented by a filled circle). All four observation points are represented by small circles in the image.

linearly polarized in the x-y plane and transmitted in the z direction, and for the remaining transmitters, the pulse is polarized in the y-z plane and transmitted in the x direction. Each observation point is located in the Scattered Field at a distance of 74 mm from the center of the tumour, which is located at the centre of the Total Field. The acquired backscattered recorded signals are downsampled from 1200 GHz to 75 GHz. Figure 2 shows a representation of the TF/SF grid, with the location of the origin of the first incident plane wave and respective observer point as well as the position of the tumour.

3. SPIKING NEURAL NETWORKS & GENETIC ALGORITHMS

3.1. Spiking Neural Network

The organic nervous system has inspired the development of Artificial Neural Networks (ANNs). Insights into the workings of biological

neurons indicate that computation is performed in the temporal domain and relies on the timings between spikes, rather than rate or level encodings as employed by earlier neural models [22–24]. These biological understandings have led to the development of Spiking Neural Networks (SNNs). SNNs, known as the third generation of neural network models, are more closely related to their biological counterparts compared to previous ANN generations, such as multi-layer perceptrons. SNNs, in contrast to previous models, employ transient pulses for communication and computation. Maass has demonstrated that spiking neurons are more computationally powerful than threshold-based neuron models [24] and that SNNs possess similar and often more computation ability compared to second generation multi-layer perceptrons [25]. Other works [26–28] have investigated SNN hardware implementations and have found that computation in the temporal domain can be performed more efficiently in hardware compared to employing complex non-linear sigmoidal neural models. These findings, and an increasing interest in efficient temporal computation have encouraged interest in SNNs and their application to classification and control tasks.

3.2. Genetic Algorithms

Inspired by nature, a Genetic Algorithm (GA) [29] models natural evolution through a set of computational operators. A GA is a parallel, population-based search strategy that encodes individual solutions into a data-structure known as a genome. A population of such genomes is maintained by the GA and mechanisms analogous to evolution are employed to evolve "good" solutions. Exploration of the search space is performed using a diversity introducing mutation operator while crossover (mating of two parent solutions) is employed to exploit good solution building blocks (known as genes) already in the population. Selection pressure is added through a tournament selection operator to incorporate "survival of the fittest". This bias towards selecting good solutions for further evaluation and recombination allows for the discovery of high-fitness SNN classifiers. A good review of the application of GAs to ANN training is presented in [30] while GAs have been employed to train SNNs in [31–34]. This research focuses on the evolution of SNN synaptic weights and thresholds. The GA parameters and evolutionary mechanisms employed for this research are as detailed in [35]. A comprehensive review of the application of GAs to ANN training is presented in [30] while GAs have been employed to train SNNs in [31–34, 36–38].

4. EXPERIMENTAL SETUP

4.1. Data Preprocessing

4.1.1. Discrete Wavelet Transform

The Discrete Wavelet Transform (DWT) produces wavelet coefficients which may be used as discriminant bases for classification methods. The DWT is applied to the Radar Target Signatures (RTS) and the resultant wavelet coefficients are obtained using low-pass decomposition filters. Subsequently, the low-pass band may be split again through further low-pass filters. It must be noted that for each iteration of the wavelet filters, the number of samples for the next stage is halved through signal decimation. This process continues to a desired number of levels. In this paper, the chosen wavelet is *Coiflet 5* (established as the optimum wavelet by empirical analysis). The frequency band that is used for classification corresponds to the wavelet coefficients obtained from the low-pass band after a two-level decomposition, as these wavelet coefficients were found to give the best classification performance compared to other subbands, evaluated up to four levels of decomposition.

4.1.2. T-Test, Normalization and Separation of data

To identify the most relevant DWT coefficients for input to the SNN, a statistical analysis was performed on the dataset to identify the DWT components that exhibit the most statistically significant differences between the malignant and benign tumours. To investigate whether the DWT coefficients for both malignant and benign tumours are normally distributed, a Kolmogorov-Smirnov test was performed on the data. This test verified that both malignant and benign tumour coefficients conform to a normal distribution. This normality result enables the use of a t-test for identifying the DWT components that exhibit the greatest statistical difference between malignant and benign tumours. A t-test identifies the largest significant differences between the means of two independent sample groups, while taking the variances of both groups into account. The independent variable is whether the tumour is malignant or benign, while the dependent variable is the level of the DWT output. The 15 DWT components that exhibit the greatest differences between malignant and benign were identified, normalised and employed for classification purposes. This process ensures that the DWT components that contain the most relevant tumour information are employed to differentiate between malignant and benign.

SNNs translate real world scalar data into spike train frequencies [39]. In this research, high DWT values correspond to high spike-train frequencies while low DWT values correspond to low frequencies. As the DWT coefficients, after normalisation, are scaled between $[-1, +1]$, it is necessary to decouple the positive and negative ranges of each DWT component ($D(n)$) into two spike generating inputs ($Dn+$ and $Dn-$). This separation ensures that a $+1$ DWT input generates the same number of spikes (and influence) on the SNN as a -1 DWT input, thus removing any bias from the encoding process.

4.2. SNN Breast Cancer Classifier System Architecture Application

Figure 3 illustrates the SNN architecture used to implement the SNN breast cancer classifier. The single-hidden-layer SNN processes the 15 most relevant DWT components (D1–D15). DWT data is translated into spike trains by spike generators (SG1-SG30) using a linear magnitude to (spike train) frequency conversion [39]. This DWT spike data is fed to the network's 30 hidden layer neurons (N1-N30). Two output layer spiking neurons (N31, N32) generate two spike train outputs which determine the system's classification. Two spike counters (SC1, SC2) are employed to count the number of spikes output from each output neuron (within a given sampling interval). Counter values C1 and C2 are used to determine classifier behaviour. The counter with the largest spike count value designates the selected class. A leaky integrate and fire neuron model [24] is employed for these experiments.

Each SNN is composed of 32 genes, which correspond to the 32 evolvable spiking neurons (N1-N32). A GA is used to evolve and train each spiking neuron's parameters. Each gene comprises 33 real-valued
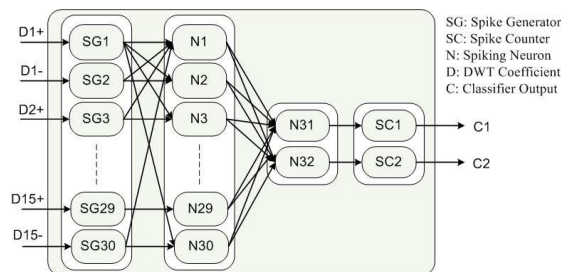

Figure 3. SNN fully-connected architecture for tumour classification. A single hidden layer, 30 DWT inputs and two classification outputs are also illustrated.

numbers (32 synaptic weights and 1 neuron firing threshold), meaning that an individual's entire genome consists of 1056 real-valued entries.

Synaptic weights vary between $[-1.05, 1.05]$ while thresholds range from $[0, 4.0]$ [35]. A fitness function is employed to perform assessment of the SNN-based breast cancer classifier. This function rewards individuals based on the number of correct classifications made. C^m refers to the number of correct malignant classifications made, while C^b refers to the number of correct benign classifications. $C_{\max}$ and $C_{\min}$ are defined in Equations (3) and (4).

$$C_{\max} = \max[C^m, C^b] \tag{3}$$

$$C_{\min} = \min[C^m, C^b] \tag{4}$$

The fitness, f, of the SNN is defined in Equation (5).

$$f = ((C_{\min})^{\beta}) + C_{\max} \tag{5}$$

To reward the correct classification of both tumour classes, a β value of 1.3 is employed. This β parameter incorporates a fitness bias which rewards individuals that achieve a more balanced classification performance across both malignant and benign tumours. Without this fitness bias, fitness can be accumulated easily by classifying a single tumour class repeatedly, without regard to the tumours DWT profile. This effortless accumulation of fitness misleads the GA in the early stages of search, since it is initially easier to gather fitness through a blind approach than to achieve a balanced fitness score by classifying both tumour types correctly. This bias therefore ensures that SNNs which select correctly from both classes are rewarded above networks that correctly select from just one class.

5. RESULTS AND CONCLUSIONS

5.1. Comparison of SNN and LDA Classifiers in a Dielectrically Heterogeneous Breast

A total of 160 tumour models were considered (80 of size 2.5 mm and 80 of size 7.5 mm). Within that group, there were 80 type 1 tumours (malignant), 40 type 2 tumours (macrolobulated benign) and 40 type 3 tumours (smooth benign). Two different classifier architectures are considered:

(i) A direct "type" classifier that simply classifies each tumour as either benign or malignant

(ii) A two-stage classifier that classifies each tumour as either small or large, before classifying the tumour as either benign or malignant.

Table 1. Comparison of LDA and SNN classifiers.

Classifier	One-Stage Type (%)	Size (%)	Small (%)	Large (%)
LDA	73	74.34	90.40	96.57
SNN	73	100	100	100

The tumour backscatter is classified using the SNN, but also using Linear Discriminant Analysis (LDA) [14], providing a useful baseline when examining the performance and robustness of the SNN classifier. In order to evaluate both classification methods, the entire data-set is randomly shuffled and divided into 75% (120 Tumours) and 25% (40 Tumours) training and test groups respectively. The classification process is repeated 10 times and the average performance of each classifier is calculated. The results are presented in Table 1. Across all tests (dielectrically homogeneous and heterogeneous), the SNN was shown to equal or significantly outperform the LDA classifier. The SNN was shown to provide 100% classification accuracy using the two-stage classifier when the tumours were first pre-classified by size.

5.2. Effects of Dielectric Heterogeneity

In order to examine the effect of increasing dielectric heterogeneity on the performance of the SNN classifier, two specific scenarios are considered. In the first instance, a single piece of fibroglandular tissue surrounds the tumour, while in the second more difficult scenario two separate pieces of fibroglandular tissue are located around the tumour. The performance of the classifier in an increasingly heterogeneous environment is shown in Table 2. The performance of the SNN classifier drops by 10 and 8.5% for one-stage type and pre-size classified large tumours as heterogeneity increases. Overall, the SNN classifier is shown to be relatively robust to significant increases in dielectric heterogeneity. In fact, in the most dielectrically heterogeneous models (Hetero II), the average performance (across large and small tumours) of the two-stage SNN classifier was over 86%.

5.3. Combining Results from Different Antennas

Four antenna elements surround the breast/tumour model. Each of these antennas record the Radar Target Signature, which is later used to classify the tumour as either benign or malignant. Often the classification results obtained from different antennas conflict (e.g., three antennas classify the tumour as benign while one antenna classifies the tumour as malignant). In this section, methods of

Table 2. Effects of dielectric heterogeneity on performance of SNN classifier. Hetero I refers to models containing one piece of fibroglandular tissue, while Hetero II refers to models with two pieces of fibroglandular tissue.

Classifier	One-Stage Type (%)	Size (%)	Small (%)	Large (%)
Hetero I	78	100	100	82
Hetero II	68	100	100	73.5

Table 3. The performance, sensitivity and specificity of the SNN classifier, illustrating the effects of combining conflicting readings.

Malignant Readings Required	Performance (%)	Sensitivity (%)	Specificity(%)
1	98	100	95.76
2	94	99.37	89.33
3	94.5	97.66	89.61
4	90	94.31	85.11

Table 4. Misclassified tumours for one-stage type classifier.

Classifier	SM (%)	SB (%)	LM (%)	LB (%)
One Stage	17.98	22.66	23.02	36.33
Two Stage	0	0	37.74	62.25

combining these conflicting results are investigated in order to produce the optimum classification algorithm in terms of both sensitivity and specificity.

The entire classification process is completed four times. Initially, only one malignant reading is required to classify the tumour as malignant. Next two malignant readings are required, followed by three readings and in the final test, all four readings must be malignant before the tumour is classified as malignant. The performance, sensitivity and specificity for each case are shown in Table 3 (for clarity only the performance of the single-stage type classifier is shown). Examining Table 3, it appears that if just one antenna signal is classified as malignant, then the tumour should be classified as malignant (ignoring the other benign readings), to provide the optimum classifier performance in terms of both sensitivity and specificity. This may be due to scenarios where the tumour spicules are concentrated on one side of the tumour and are therefore only "visible" to one antenna. Choosing a threshold of one malignant

reading therefore ensures a high sensitivity (resulting in less false-negative results) and a high specificity (resulting in less false-positive results).

5.4. Analysis of Misclassified Tumours

It is important to consider which tumours are being misclassified by the SNN classifier. The misclassified tumours from the one and two-stage type classifier are divided into four categories: Small Malignant (SM), Small Benign (SB), Large Malignant (LM) and Large Benign (LB), and are shown in Table 4. Examining the one-stage classifier, the tumour type most often misclassified was Large Benign (LB). The remainder of the misclassified tumours were distributed relatively evenly across the other three categories. Significantly, in the two-stage classifier, the Large Benign was once again the largest misclassified category. In the one-stage classifier, it appears that the Large Benign tumours are often misclassified as either Large Malignant or Small Malignant. This reinforces the need of a two-stage classifier, where the tumours are pre-classified by size. In the two stage classifier, a Large Benign tumour can no longer be misclassified as a Small Benign.

In the two-stage classifier, the misclassifications occur only between Large Benign and Large Malignant tumour types. This may well be caused by the tumour modeling process. Across all malignant tumours, fixed length cones are used to model tumour spicules. In the smaller tumour models, these cones protrude much further from the spherical surface of the tumour compared to the large tumour models. Therefore, there would be a much greater difference in the RTS of benign and malignant small tumours, rather than benign and malignant large tumours.

6. CONCLUSIONS

The performance of an SNN classifier in a dielectrically heterogeneous breast was examined in this paper. A large database of breast models was created, containing GRS tumour models and dielectric heterogeneity extracted from the UWCEM breast phantom repository. The SNN was shown to significantly outperform the LDA classifier in the dielectrically heterogeneous models. The SNN classifier was also shown to be relatively robust to increasing levels of heterogeneity within the breast. It must be noted that the performance and robustness of the classifier may partly be attributed to the fact that the tumour is positioned at a fixed location at the centre of the breast. Because the tumour position is fixed across all models, the classifier can

more easily isolate the portion of the RTS influenced by the shape and size of the tumour and effectively ignore any surrounding heterogeneity. Future work will examine the performance of the classifier when the tumour (and heterogeneity) is randomly located within the breast.

The effect of combining conflicting readings from different antennas was considered. The optimum approach (in terms of sensitivity and specificity) was to classify the tumour as malignant if any one of the antenna readings was classified as malignant. This was most likely due to scenarios where the spicules from malignant tumours all protrude in the same general direction and only had a significant effect on the RTS received at one antenna.

The misclassified tumours were examined and considered. The most common type of tumour misclassified was large benign. This tumour was often misclassified as either large malignant or small malignant, highlighting the need for pre-size classification step. When the tumours were size-classified (in the two stage classifier), large benign was once again the most often misclassified tumour. This may be attributed to the tumour modeling process where fixed-length spicules were used. These spicules protruded much further from the surface of smaller tumours than from the larger tumours, making it more difficult to differentiate between the RTS of large benign and malignant tumours. This issue with the tumour models will be examined in a future study.

ACKNOWLEDGMENT

REFERENCES

1. Nass, S. L., I. C. Henderson, and J. C. Lashof, *Mammography and Beyond: Developing Technologies for the Early Detection of Breast Cancer*, National Academy Press, 2001.

2. Bird, R. E., T. W. Wallace, and B. C. Yankaskas, "Analysis of cancers missed at screening mammograph," *Radiology*, Vol. 184, 613–617, 1992.

3. Huynh, P. H., A. M. Jarolimek, and S. Daye, "The false-negative mammogram," *RadioGraphics*, Vol. 18, 1137–1154, 1998.

4. Elmore, J. G., M. B. Barton, V. M. Moceri, S. Polk, P. J. Arena, and S. W. Fletcher, "Ten-year risk of false positive screening mammograms and clinical breast examinations," *New Eng. J. Med.*, Vol. 338, No. 16, 1089–1096, 1998.

5. Hall, F. M., J. M. Storella, D. Z. Silverstone, and G. Wyshak, "Non-palpaple breast-lesions, recommendations for biopsy based on suspicion of carcinoma at mammography," *Radiology*, Vol. 167, No. 2, 353–358, 1988.

6. Zainud-Deen, S., W. Hassen, E. Ali, and K. Awadalla, "Breast cancer detection using a hybrid finite difference frequency domain and particle swarm optimization techniques," *Progress In Electromagnetics Research B*, Vol. 3, 35–46, 2008.

7. AlShehri, S. and S. Khatun, "UWB imaging for breast cancer detection using neural network," *Progress In Electromagnetics Research C*, Vol. 7, 79–93, 2009.

8. Maskooki, A., E. Gunawan, C. Soh, and K. Low, "Frequency domain skin artifact removal method for ultra-wideband breast cancer detection," *Progress In Electromagnetics Research*, Vol. 98, 299–314, 2009.

9. Conceição, R. C., D. Byrne, M. O'Halloran, M. Glavin, and E. Jones, "Comparison of planar and circular antenna configurations for breast cancer detection using microwave imaging," *Progress In Electromagnetics Research*, Vol. 99, 1–19, 2009.

10. Nguyen, M. and R. Rangayyan, "Shape analysis of breast masses in mammograms via the fractial dimension," *27th Annual Conference of the IEEE Engineering in Medicine and Biology*, 3210–3213, 2005

11. Chen, Y., I. Craddock, and P. Kosmas, "Feasibility study of lesion classification via contrast-agent-aided uwb breast imaging," *IEEE Transactions on Biomedical Engineering*, Vol. 57, No. 5, 1003–1007, 2010.

12. Chen, Y., I. Craddock, P. Kosmas, M. Ghavami, and P. Rapajic, "Application of the mimo radar technique for lesion classification in UWB breast cancer detection," *17th European Signal Processing Conference (EUSIPCO)*, 759–763, 2009.

13. "Multiple-input multiple-output radar for lesion classification in ultrawideband breast imaging," *IEEE Journal of Selected Topics in Signal Processing*, Vol. 4, No. 1, 187–201, 2010.

14. Conceição, R. C., D. Byrne, M. O'Halloran, E. Jones, and M. Glavin, "Investigation of classifiers for early-stage breast cancer based on radar target signatures," *Progress In Electromagnetics Research*, Vol. 105, 295–311, 2010.

15. Conceição, R. C., M. O'Halloran, M. Glavin, and E. Jones, "Support vector machines for the classification of early-stage breast cancer based on radar target signatures," *Progress In*

Electromagnetics Research B, Vol. 23, 311–327, 2010.

16. Davis, S. K., B. D. V. Veen, S. C. Hagness, and F. Kelcz, "Breast tumor characterization based on ultrawideband backscatter," *IEEE Trans. Biomed. Eng.*, Vol. 55, No. 1, 237–246, 2008.

17. Muinonen, K., "Introducing the gaussian shape hypothesis for asteroids and comets," *Astronomy and Astrophysics*, Vol. 332, 1087–1098, 1998.

18. Muinonen, K., *Light Scattering by Stochastically Shaped Particles*, Chapter 11, Academic Press, 2000.

19. Lazebnik, M., L. McCartney, D. Popovic, C. B. Watkins, M. J. Lindstrom, J. Harter, S. Sewall, A. Magliocco, J. H. Booske, M. Okoniewski, and S. C. Hagness, "A large-scale study of the ultrawideband microwave dielectric properties of normal breast tissue obtained from reduction surgeries," *Phys. Med. Biol.*, Vol. 52, 2637–2656, 2007.

20. Lazebnik, M., D. Popovic, L. McCartney, C. B. Watkins, M. J. Lindstrom, J. Harter, S. Sewall, T. Ogilvie, A. Magliocco, T. M. Breslin, W. Temple, D. Mew, J. H Booske, M. Okoniewski, and S. C. Hagness, "A large-scale study of the ultrawideband microwave dielectric properties of normal, benign and malignant breast tissues obtained from cancer surgeries," *Phys. Med. Biol.*, Vol. 52, 6093–6115, 2007.

21. Taflove, A. and S. C. Hagness, *Computational Electrodynamics: The Finite-difference Time-domain Method*, Artech House Publishers, June 2005.

22. Maass, W., "Computation with spiking neurons," *The Handbook of Brain Theory and Neural Networks*, 1080–1083, 2003.

23. Gerstner, W. and W. Kistler, *Spiking Neuron Models*, Cambridge University Press, New York, 2002.

24. Maass, W., "Networks of spiking neurons: The third generation of neural network models," *Neural Networks*, Vol. 10, No. 9, 1659–1671, 1997.

25. Maass, W., "Computing with spiking neurons," *Pulsed Neural Networks*, MIT Press, 85, 1999.

26. Maguire, L., T. McGinnity, B. Glackin, A. Ghani, A. Belatreche, and J. Harkin, "Challenges for large-scale implementations of spiking neural networks on FPGAs," *Neurocomputing*, Vol. 71, Nos. 1–3, 13–29, 2007.

27. Floreano, D., N. Schoeni, G. Caprari, and J. Blynel, "Evolutionary bits'n'spikes," *Artificial Life Eight*, 335, 2003.

28. Morgan, F., S. Cawley, B. McGinley, S. Pande, L. McDaid,

B. Glackin, J. Maher, and J. Harkin, "Exploring the evolution of NoC-based spiking neural networks on FPGAs," *IEEE International Conference on Field-programmable Technology, 2009 FPT*, 300–303, 2010.

29. Holland, J., *Adaptation in Natural and Artificial Systems*, MIT Press, Cambridge, MA, 1992.

30. Yao, X., "Evolving artificial neural networks," *Proceedings of the IEEE*, Vol. 87, No. 9, 1423–1447, 1999.

31. Hagras, H., A. Pounds-Cornish, M. Colley, V. Callaghan, and G. Clarke, "Evolving spiking neural network controllers for autonomous robots," *IEEE International Conference on Robotics and Automation*, Vol. 5, 4620–4626, 2004.

32. Floreano, D., N. Schoeni, G. Caprari, and J. Blynel, "Evolutionary bits'n'spikes," *Proceedings of the Eighth International Conference on Artificial Life*, 335–344, 2003.

33. Belatreche, A., L. P. Maguire, M. McGinnity, and Q. X. Wu, "Evolutionary design of spiking neural networks," *New Mathematics and Natural Computation (NMNC)*, Vol. 2, No. 03, 237–253, 2006.

34. McGinley, B., M. O'Halloran, R. C. Conceicao, F. Morgan, M. Glavin, and E. Jones, "Spiking neural networks for breast cancer classification using radar target signatures," *Progress In Electromagnetics Research C*, Vol. 17, 79–94, 2010.

35. Rocke, P., B. McGinley, J. Maher, F. Morgan, and J. Harkin, "Investigating the suitability of FPAAs for evolved hardware spiking neural networks," *Proceedings of Evolvable Systems: From Biology to Hardware*, 118–126, 2008.

36. Kasabov, N., *Evolving Connectionist Systems: The Knowledge Engineering Approach*, Springer-Verlag Inc., New York, 2007.

37. Kasabov, N., "Integrative connectionist learning systems inspired by nature: Current models, future trends and challenges," *Natural Computing*, Vol. 8, No. 2, 199–218, 2009.

38. Schliebs, S., M. Defoin-Platel, S. Worner, and N. Kasabov, "Integrated feature and parameter optimization for an evolving spiking neural network: Exploring heterogeneous probabilistic models," *Neural Networks*, Vol. 22, Nos. 5–6, 623–632, 2009.

39. Pande, S., F. Morgan, S. Cawley, B. McGinley, S. Carrillo, L. McDaid, and J. Harkin, "Embrace-sysc for analysis of noc-based spiking neural network architecture," *IEEE System on a Chip Symposium (SOC)*, 2010.